Bioactive Materials 11 (2022) 230–239

Contents lists available at ScienceDirect

Bioactive Materials

journal homepage: www.keaipublishing.com/en/journals/bioactive-materials

Nanocomposite electrospun fibers of poly(ε-caprolactone)/bioactive glass with shape memory properties

Liliana Liverani [a,*,1], Anna Liguori [b,1], Paola Zezza [b], Chiara Gualandi [b,c], Maurizio Toselli [d], Aldo R. Boccaccini [a], Maria Letizia Focarete [b,e,**]

[a] Institute of Biomaterials, Department of Materials Science and Engineering, University of Erlangen-Nuremberg, Cauerstr. 6, 91058, Erlangen, Germany
[b] Department of Chemistry "Giacomo Ciamician" and INSTM UdR of Bologna, University of Bologna, via Selmi 2, 40126, Bologna, Italy
[c] Interdepartmental Center for Industrial Research on Advanced Applications in Mechanical Engineering and Materials Technology, CIRI-MAM, University of Bologna, Viale Risorgimento, 2, 40136, Bologna, Italy
[d] Department of Industrial Chemistry "Toso Montanari", University of Bologna, Viale Risorgimento 4, 40136, Bologna, Italy
[e] Health Sciences and Technologies – Interdepartmental Center for Industrial Research (HST-ICIR), Alma Mater Studiorum - Università di Bologna, 40064, Ozzano dell'Emilia, Bologna, Italy

ARTICLE INFO

Keywords:
PCL-TES
Bioactive glasses
Bioactivity
Shape memory polymers
Electrospinning
Benign solvents

ABSTRACT

Electrospun fibers of shape memory triethoxysilane-terminated poly(epsilon-caprolactone) (PCL-TES) loaded with bioactive glasses (BG) are here presented. Unloaded PCL-TES, as well as PCL/BG nanocomposite fibers, are also considered for comparison. It is proposed that hydrolysis and condensation reactions take place between triethoxysilane groups of the polymer and the silanol groups at the BG particle surface, thus generating additional crosslinking points with respect to those present in the PCL-TES system. The as-spun PCL-TES/BG fibers display excellent shape memory properties, in terms of shape fixity and shape recovery ratios, without the need of a thermal crosslinking treatment. BG particles confer *in vitro* bioactivity to PCL-based nanocomposite fibers and favor the precipitation of hydroxycarbonate apatite on the fiber surface. Preliminary cytocompatibility tests demonstrate that the addition of BG particles to PCL-based polymer does not inhibit ST-2 cell viability. This novel approach of using bioactive glasses not only for their biological properties, but also for the enhancement of shape memory properties of PCL-based polymers, widens the versatility and suitability of the obtained composite fibers for a huge portfolio of biomedical applications.

1. Introduction

The fabrication of tissue engineering scaffolds based on the use of shape memory polymers (SMPs) attracted the interest of the scientific community in the last decades. SMPs, investigated for the first time in the 1980s, are a class of stimuli-responsive polymers that can return to their initial permanent shape from a temporary programmed one after exposure to an external stimulus (i.e. temperature variation, solvent hydration, electric and magnetic field) [1–4]. SMPs are suitable for several biomedical applications [4–8], including the fabrication of clot removal devices, aneurysm occlusion devices, stents, devices for cardiac valve repair, occluders for congenital heart disease, orthodontics applications, and scaffolds for tissue engineering. In the latter case, SMPs have been proposed for the engineering of bone [9–13], cartilage [14], cardiovascular system [15,16], and trachea [17] as well as for the smart delivery of therapeutic agents [18–21]. Apart from their basic capability of permitting minimally invasive surgical implantation [4], SMPs have emerged as suitable materials for the fabrication of scaffolds or implants whose shape can be properly tuned immediately before or during their implantation, in order to perfectly fit with the dimensions and geometries of the portion of the tissue to be regenerated [9]. Properly crosslinked PCL-based scaffolds are particularly exploitable for this application. Indeed, showing a T_m above the human body temperature, when heated above this temperature they become malleable and

Peer review under responsibility of KeAi Communications Co., Ltd.
* Corresponding author.
** Corresponding author. Department of Chemistry "Giacomo Ciamician" and INSTM UdR of Bologna, University of Bologna, via Selmi 2, 40126, Bologna, Italy.
E-mail addresses: liliana.liverani@fau.de (L. Liverani), marialetizia.focarete@unibo.it (M.L. Focarete).
[1] These authors have contributed equally to this work and share first authorship.

https://doi.org/10.1016/j.bioactmat.2021.09.020
Received 21 May 2021; Received in revised form 8 September 2021; Accepted 9 September 2021
Available online 23 September 2021

their shape can be easily modified. Upon cooling, the crystallization of the PCL domains causes the scaffolds to return to their rigid state, fixing the conferred shape, which is maintained also after implantation in the human body. This strategy would enable to solve many practical problems, such as scaffold shape/position maintenance in the body and, through the combination with specific bioactive functionalities, shape-memory scaffolds favoring the tissue regeneration can be obtained. Moreover, a better fitting of the scaffold to the patients defect shape and size could be achieved with this approach. Different bioactive agents have been incorporated into SMPs, including hydroxyapatite [22–24], polydopamine [9], proteins [24] and chondrogenic molecules [14]. An additional advantage of SMPs is their easy processability, enhancing their possibility of applications. Most of the scaffold fabrication techniques used with SMPs are related to electrospinning [10,18,25–29], microsphere fabrication [12,13,30] and 3D or 4D printing [17,31]. Focusing on electrospinning, examples of processable SMPs are shape memory polyurethane (SMPU) block copolymers [32–34], degradable polyesterurethane multiblock copolymer consisting of crystallizable poly(ω-pentadecalactone) and poly(ε-caprolactone) [35], α,ω-triethoxysilane-terminated poly(ε-caprolactone) [25,26], dimethacrylate poly(ε-caprolactone) [36], dimethacrylate poly(lactic acid) (PLA) and poly(vinyl acetate) (PVAc) [27]. Typical solvents involved in the process are tetrahydrofuran, dichloromethane, chloroform, *N*, *N*-dimethylformamide. Although electrospun fibers generally retain solvents only in traces, these can be definitely eliminated only by applying post-treatments, therefore, for the purpose of biomedical application the use of benign solvents for electrospinning is highly desired [37,38]. Motivated by the unique biomimetic morphological properties displayed by electrospun scaffolds, combined with the versatility of the technology that allows the incorporation of bioactive inorganic micro and nanosized particles inside fibers, we propose to incorporate bioactive glasses into shape memory fibers to develop a biomimetic, bioactive and shape-programmable osteogenic scaffold, using a benign solvent for the electrospinning process.. PCL-based electrospun composite fibers (without shape memory properties) containing bioactive glass particles have been already obtained by using both neat PCL and its blends with different natural and synthetic polymers [39–41].

In this work, we used the biodegradable and bioresorbable PCL, properly modified at chain-ends, to generate, via sol-gel chemistry, SiO_2 domains that act as permanent crosslinking points for shape recovery. Indeed, we previously demonstrated that the triethoxysilane-terminated PCL (PCL-TES) can be electrospun and exhibits shape memory properties with a T_{trans} corresponding to the melting temperature of PCL (about 55 °C) [25,26]. Furthermore, to endow the scaffolds with bioactive functionalities, in the present study, we selected bioactive glasses (BGs) [42], which are well-known for their capability to bind the host tissue by forming a layer of hydroxycarbonate apatite on their surface (bioactivity). BGs show excellent osteoinductivity, antibacterial properties, capability to modulate angiogenesis, inflammatory process, and several other effects induced by the release of therapeutic ions suitable for bone and soft tissue engineering [43–46]. For this reason, the use of bioactive glasses for the fabrication of composite scaffolds, in particular in combination with polyesters (as PCL), also with the aim to improve scaffold properties as hydrophilicity and apatite forming ability, has been already reported in the last decades [47,48]. Beside the addition of those functionalities, in this work, we used BGs to exploit the formation of chemical interactions between the silanol groups at the particle surface and PCL-TES chain ends. It is thus expected that the chemical reactivity between the shape memory polymer and the inorganic additive will facilitate particle dispersion and will have an effect over shape memory properties. Electrospun fibers of crosslinked shape memory PCL-TES loaded with chemically reactive BGs have been fabricated by using benign solvents and characterized in their shape memory performances, incorporation of BG particles, acellular bioactivity and preliminary cytocompatibility. Unloaded shape memory PCL-TES fibers, as well as PCL/BG nanocomposites, were also considered for comparison.

2. Materials and methods

Materials: Poly(ε-caprolactone) (PCL) (M_n = 80000 g mol^{-1}, Sigma Aldrich) and glacial acetic acid 99.85% (VWR, Germany) were used for the electrospinning process of the neat uncrosslinked polymer. α,ω-Triethoxysilane-terminated poly(ε-caprolactone) (PCL-TES) was synthesized starting from an α,ω-Hydroxyl-terminated poly(ε-caprolactone) (M_n = 10000 g mol^{-1}) and 3-(triethoxysilyl)propyl isocyanate (ICPTS), purchased from Sigma-Aldrich and used as received, according to the procedure reported by Paderni et al. [49] For the fabrication of the composite fibers, commercially available bioactive glass particles 45S5 (Schott Vitryxx®), with composition 45 wt% SiO_2, 24.5 wt% CaO, 24.5 wt% Na_2O, and 6.0 wt% P_2O_5 and nominal mean particle size of 2 μm, were purchased from Schott AG (Germany) and used as received.

Electrospinning: Electrospinning was carried out by using a commercially available apparatus (Starter Kit 40 KV Web, Linari srl, Italy), comprised of a high-voltage power supply, a syringe pump, a syringe, a stainless steel blunt-ended needle (inner diameter 0.51 mm) connected with the power supply electrode and a grounded aluminum foil. PCL electrospun scaffolds were produced by dissolving the polymer at a concentration of 20% w/v in glacial acetic acid, according to the protocol previously reported by Liverani et al. [39]. Electrospun scaffolds of neat PCL-TES were produced by dissolving the polymer at a concentration of 35% w/v in glacial acetic acid and left under stirring overnight at room temperature (RT). BG particles were dispersed in the polymeric solution with a concentration of 30 wt% with respect to the polymer content (corresponding to a 23 wt% of the total weight), after constant stirring for 10 min. The suspensions containing PCL (or PCL-TES) and BG particles were stable, without any visible precipitates. The stirring time and the electrospinning time were limited to 10 min for each step, according to previously optimized protocols [39–41].

For all solutions and suspensions, the optimized process parameters for electrospinning are summarized in Table 1. The electrospinning process was carried out at 24 °C and 40% of relative humidity. Electrospun meshes were maintained under vacuum at 4 °C until their characterization.

Post-crosslinking: The post-crosslinking treatment was performed to increase the crosslinking density in PCL-TES and PCL-TES/BG scaffolds for enhancing their shape memory properties [25]. It consisted in storing the electrospun mat at 40 °C for 72 h in the presence of an acid environment. PCL-TES and PCL-TES/BG scaffolds were hanged to a glass rod at the top of a beaker (200 mL). The beaker was filled with 100 mL of distilled water and 3 mL of HCl 37% (Sigma Aldrich). The mats were not in direct contact with the acid solution but only with its acidic vapors.

Gel content: Specimens of PCL-TES and PCL-TES/BG, as-spun and post-crosslinked, were weighed to get their initial weight (m_0) and then immersed in dichloromethane (DCM) (15 mL). After 17 h, the DCM was refreshed and after additional 2 h the excess of DCM was removed from

Table 1
Polymer concentration and electrospinning operating parameters for each solution.

Sample	Polymer concentration [w/v %]	BG content[a] [w/w %]	Applied voltage [kV]	Distance needle-target [cm]	Flow rate [mL/h]
PCL	20	0	15	11	0.4
PCL-TES	35	0	20	15	2
PCL/BG	20	30	15	11	0.8
PCL-TES/BG	30	30	15	10	2

[a] BG weight over polymer weight.

the samples. The swollen samples were dried at RT overnight in order to determine the residual mass (m_d) after the dissolution of non-crosslinked PCL-TES macromolecules. The gel content (G) was calculated according to Equation (1):

$$G = \frac{m_d - f_{BG} m_0}{f_{PCL-TES} m_0} \times 100 \quad (1)$$

Where f_{BG} and $f_{PCL\text{-}TES}$ are the weight fractions of BG and PCL-TES measured by TGA, respectively. Gel content was measured on three replicates for each sample and results were provided as average ± standard deviation.

Characterization techniques: Fiber morphology and local elemental composition were investigated by SEM analysis, using the microscope Auriga Base (Carl Zeiss, Germany), equipped with an EDX modulus; samples were gold sputtered before the analysis using a sputter coater (Q150T, Quorum Technologies). Fiber average diameters were calculated using ImageJ analysis software (NIH, USA) [50], after the measurement of 30 fibers from each sample. Transmission Electron Microscopy (TEM) observations were also carried out on as-spun samples containing BG by using a Philips microscope with an acceleration voltage of 80 kV.

Thermograms were acquired by means of a TGA Q500 (TA Instruments), under air atmosphere, by heating the sample from RT to 600 °C with a rate of 10 °C/min; analysis was carried out by placing the sample in a platinum pan with a weight range of 5–10 mg.

Calorimetric analysis of the electrospun mat was carried out with a DSC Q2000 (TA Instruments), equipped with a Liquid Nitrogen Cooling system (LNCS). Analyses were carried out under a 50 mL/min helium flow; the thermal program consisted in a first heating from −100 °C to 100 °C at a heating rate of 20 °C/min, a controlled cooling at 10 °C/min followed by a second heating scan. The DSC traces enabled to assess the glass transition (T_g) and the melting (T_m) temperatures of the produced mats; the crystallinity content (χ_c) was also determined by using Equation (2):

$$\chi_c = \frac{\Delta H_m}{f \Delta H_m^0} \times 100 \quad (2)$$

Where ΔH_m is the melting enthalpy of either PCL or PCL/TES, f is the weight fraction of the polymer and ΔH_m^0 is the melting enthalpy of the 100% crystalline PCL (134.9 J/g [51]).

One-way shape memory test: The shape memory behavior of the electrospun scaffolds was studied using a DMA Q800 (TA Instruments, New Castle, Delaware, U.S.A.) in tensile configuration. The specimens were cut into rectangular strips (gauge length: 8 mm; width: 5 mm, thickness: in the range 0.1–0.2 mm) and were preliminarily subjected to a thermal treatment consisting of heating the specimen at 85 °C, where the samples were allowed to shrink until a constant length was obtained. This treatment was necessary to gain samples with dimensional stability [25,52]. A thermo-mechanical loading-unloading cycle was then applied to assess shape memory properties, consisting in: (i) heating the specimen up to 80 °C, i.e. above polymer T_m, under a constant stress of 7 kPa; (ii) deforming the specimen at 80 °C by applying a deformation of about 150%, under load control (loading rate: 0.04 N min^{-1}) to get the temporary shape (programming step); (iii) fixing the temporary shape by cooling the sample under fixed strain condition to 0 °C, and the unloading (fixing step); (iv) monitoring the shape recovery during a heating ramp at 3 °C/min up to 80 °C under a constant load of 0.007 N (recovering step). The shape memory behavior was described in terms of shape fixity ratio (R_f, Equation (3)), which quantifies the amount of the applied strain fixed at the end of the cooling step, and shape recovery ratio (R_r, Equation (4)), representing the amount of applied strain recovered by the specimen after heating to 80 °C and, thus, the ability to recover its permanent shape. These parameters were calculated as follows:

$$\textit{Shape fixity}\ (\%) = R_f = \frac{\varepsilon_{unload}}{\varepsilon_{applied}} \times 100 \quad (3)$$

$$\textit{Shape recovery}\ (\%) = R_r = \frac{\varepsilon_{applied} - \varepsilon_{res}}{\varepsilon_{applied} - \varepsilon_0} \times 100 \quad (4)$$

where $\varepsilon_{applied}$ is the applied deformation (at the end of the programming step), ε_{unload} is the strain after load removal (at the end of the fixing step), ε_{res} is the residual strain measured after the recovering step, and ε_0 is the strain before deformation.

Acellular in vitro bioactivity: The *in vitro* bioactivity of the electrospun fibers was evaluated by investigating possible hydroxycarbonate apatite formation on the surface of the fiber during their immersion in simulated body fluid (SBF), properly prepared according to the procedure reported in literature [53]. This test was performed to assess any possible inhibition of the bioactivity (typical of BG particles) related to the electrospinning process, incorporation in the polymeric fibers and interaction with the SMP. Samples were cut from the meshes with a circular form and fixed on scaffold holders for 24 multiwell plate (CellCrown, Scaffdex, Sigma Aldrich) and were soaked into 15 mL of SBF at 37 °C. The amount of SBF solution was calculated accordingly to Kokubo et al. [53] After their removal from SBF, samples were gently washed with deionized water and dried at RT. The formation of apatite structures was assessed after 1 day and 7 days of immersion in SBF by combining SEM, EDX and FTIR analyses.

Biological assay: ST-2 cells (Leibniz-Institut DSMZ—German Collection of Microorganisms and Cell Cultures GmbH, Germany) were selected for their versatility for applications in hard and soft tissue engineering [54–56] for a preliminary evaluation of the cytocompatibility of PCL-TES and PCL-TES/BG electrospun fibers to assess possible effects related to the use of benign solvents and also to the presence of BG particles on the electrospun mats. Cell seeding and also the evaluation of cell adhesion and proliferation were performed according to the protocol reported by Liverani et al. [38] Briefly, ST-2 cells were cultured in RPMI 1640 medium (Thermo Fisher Scientific), containing 10% fetal bovine serum (Lonza) and 1% penicillin/streptomycin (Lonza) and then seeded on the scaffolds, previously disinfected under UV light, by drop seeding 1.5×10^4 cells (in a drop of 100 μL) per scaffold. For the cytotoxicity assessment, WST-8 assay (Cell Counting Kit-8 (CCK-8), Sigma) was performed 1 and 7 days after the seeding. Cell nuclei and cytoskeleton were stained by using rhodamine phalloidin and DAPI (Thermo Fisher Scientific) according to the protocol reported in Ref. [37] and subsequently cell morphology was evaluated by using a fluorescence microscope (Axio Scope A1, Zeiss).

3. Results and discussion

Acetic acid, classified as benign solvent [38], was used for the fabrication of nanofibrous PCL and PCL-TES meshes containing BG particles and for the controls with neat polymers. The electrospinning process parameters for PCL and PCL/BG have been optimized in a previous work [39]. In contrast, for PCL-TES formulations the previously used solvents mixture tetrahydrofuran (THF):dimethylformamide (DMF) [25,26] has been substituted with glacial acetic acid, where the water traces present in the solvent are enough to activate the hydrolysis of triethoxysilane terminal groups. The latter, through a sol-gel reaction between triethoxysilane terminal groups, contribute to increase polymer molecular weight and solution viscosity, thus enabling the obtainment of bead-free fibers, as previously demonstrated for another solvent mixture [25,26]. One main challenge faced during the preparation of PCL-TES composite fibers was the use of benign solvents for electrospinning [38], applied to SMPs. In fact, in this case acetic acid represents a sub-optimal solvent for PCL-TES and optimization was needed in terms of appropriate suspension properties to allow the electrospinnability and the determination of the process parameters.

Fig. 1 shows SEM images of the produced electrospun meshes, while

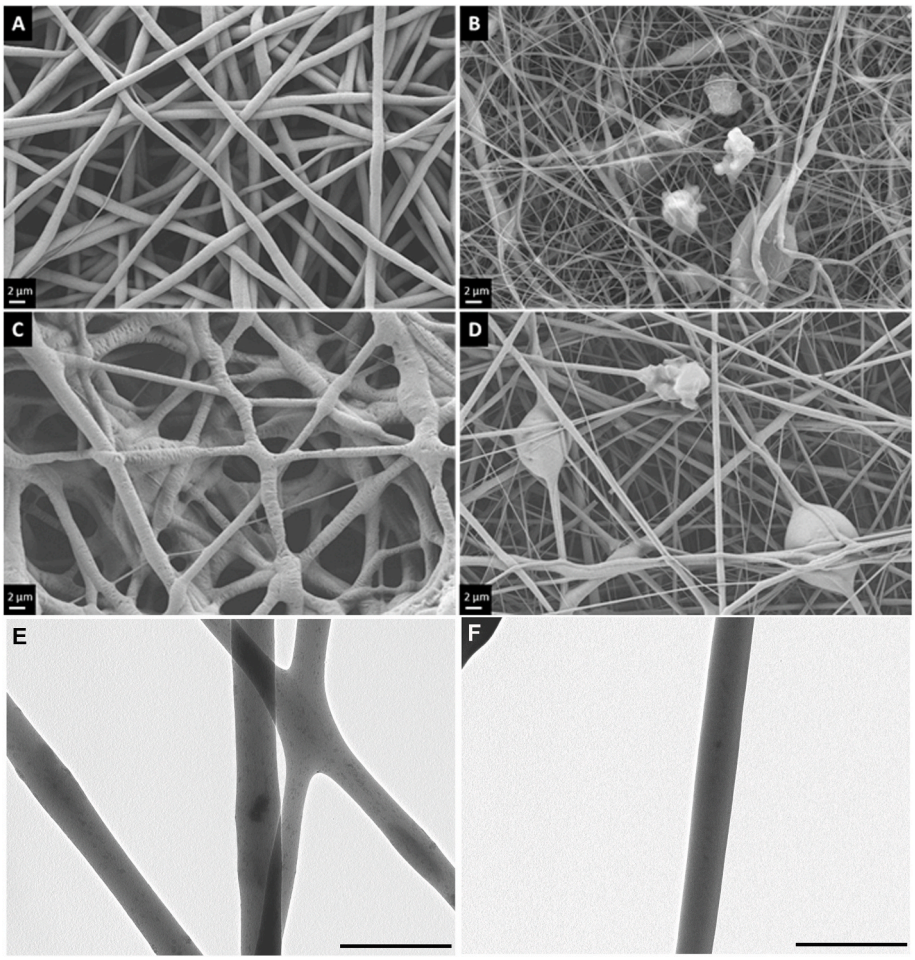

Fig. 1. SEM micrographs of the electrospun meshes obtained from glacial acetic acid solutions of (A) PCL, (B) PCL/BG, (C) PCL-TES, (D) PCL-TES/BG. Scale bars = 2 μm. TEM images of (E) PCL/BG as spun fibers, (F) PCL-TES/BG as spun fibers. Scale bars = 500 nm.

the corresponding fiber diameter distributions are reported in Fig. S1 (enclosed in Supporting Information). PCL meshes showed a homogeneous, bead- and defect-free morphology, with a mean fiber diameter of 1.2 ± 0.4 μm; PCL-TES meshes were characterized by a less uniform morphology than PCL, with a mean fiber diameter of 1.4 ± 0.4 μm. The introduction of BG particles in the polymeric solutions caused an increase of the viscosity, in particular for the PCL-TES/BG system, a decrease of the polymer concentration from 35% w/v to 30% w/v was necessary to ensure the electrospinnability of the suspension and the production of composite meshes, requiring additionally a further optimization of the electrospinning parameters. The significant increment of viscosity is probably related to the hydrolysis and condensation reactions between triethoxysilane groups of the polymer and the silanol groups at the BG particle surface, as highlighted in the scheme in Fig. 2. The optimization of the suspension composition and electrospinning parameters enabled to collect nanofibrous PCL/BG and PCL-TES/BG meshes with a mean fiber diameter of 0.3 ± 0.1 μm and 0.5 ± 0.2 μm, respectively, albeit some defects with irregular shape and rough surface are present along fibers, consistent with the presence of BG aggregates. Therefore, the addition of BG particles in both polymeric solutions has the effect of reducing the fiber diameter, ascribable to a massive change of solution properties as a consequence of the release of ions related to the BG partial dissolution. The presence of BG inside the fibers was further assessed by TEM analysis (Fig. 1E and F). Although this analysis could not be representative of the entire distribution of fiber diameters, being applicable only to fibers with diameters smaller than 200 nm, it provides reliable information about the distribution of inorganic particles in the fibers with low diameters. In both composites, the inorganic component is homogeneously distributed in the polymer matrix as particles of nanometric dimension, albeit the nominal dimension of BG particles is about 2 μm. It has to be considered that the BG particles used in the present work are characterized by numerous particles having size in the range of the declared nominal one as well as by several smaller particles, as previously reported in Ref. [39], which size could be already compatible with the reported incorporation inside the electrospun fibers. The morphological analysis of the BG particles before and after immersion in acetic acid is reported in Fig. S2.

Electrospun samples were characterized by TGA to confirm the nominal concentration of bioactive glass particles in the fibers (Fig. 3A). PCL and PCL-TES show a single weight loss at a temperature of maximum degradation rate (T_{max}) of 417 °C and 376 °C, respectively. Since the thermal degradation triggers the statistical chain cleavage in PCL, the lower thermal stability of PCL-TES compared to PCL is ascribable to its lower molecular weight, as previously reported [57]. The presence of BG in the fibers anticipates the thermal degradation of the polymer both in the case of PCL and PCL-TES, which degrades with a multi-step process. This finding can be ascribable both to the action of water entrapped in the BG particles that promotes ester hydrolysis (both samples containing BG shows a modest but not negligible weight loss from RT to 150 °C of about 0.5% ascribable to water loss, Fig. S3 in Supporting Information), and to a reaction between the ester groups of the PCL and the SiO^- groups present at the surface of bioactive glass particles, as previously reported [58]. The residual weight is correlated to the amount of BG in the fibers that was calculated by considering that:

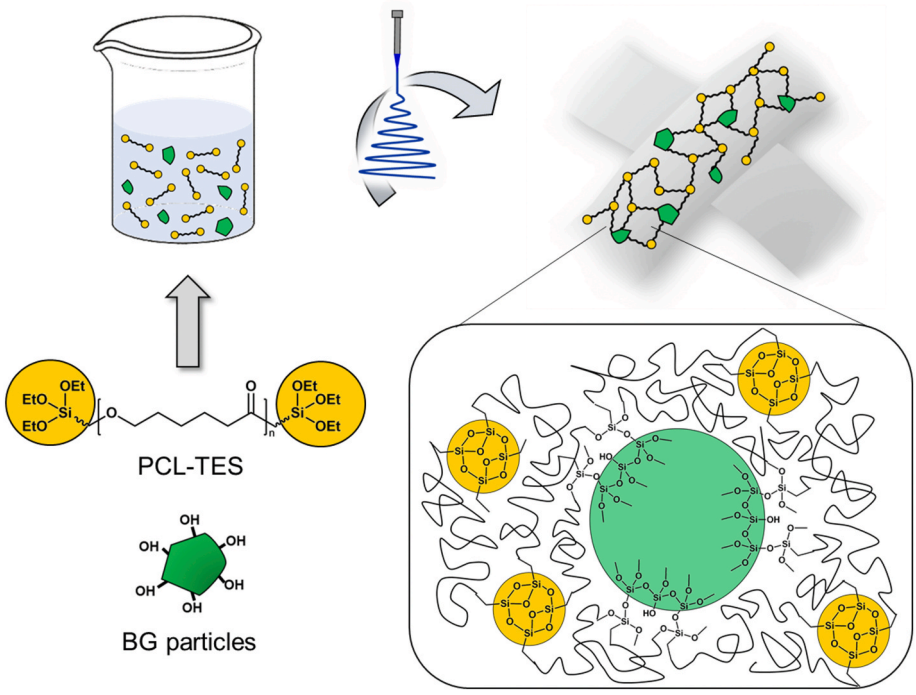

Fig. 2. Scheme of the proposed mechanism of polymer/BG binding in the PCL-TES/BG system with the formation of additional crosslinking points derived from the hydrolysis and condensation reactions of PCL-TES chain ends with BG particle surface.

(i) the polymeric component completely degrades at 600 °C and (ii) the residual weight % of BG particles is 94%. From the TGA curves, the effective BGs content is 25 wt% and 15 wt% for PCL/BG and PCL-TES/BG, respectively; this result confirms the nominal composition for PCL/BG, while for PCL-TES/BG a BG loading lower than expected was found.

DSC analysis was also carried out to evaluate the effect of bioactive glass particles loading on fiber thermal transitions. The calorimetric heating scan performed after a controlled cooling at 10 °C/min (DSC controlled cooling scan showed in Fig. S4), is reported in Fig. 3B and the corresponding calorimetric data are listed in Table 2. All samples show the typical thermal transition of polycaprolactone: a T_g around −60 °C followed by a broad melting endotherm with a T_m around 55 °C for PCL meshes and 53 °C for PCL-TES samples. The amount of crystal phase, calculated by considering the weight fraction of the polymer in the different samples, was lower in both composite meshes, with a higher decrement for PCL-TES/BG compared to PCL/BG, demonstrating that the presence of BG in the fibers slightly hinders the capability of PCL to crystallize while massively limiting the crystallization of PCL-TES. This result might be ascribed to the formation of chemical interactions between the PCL-TES chain ends and the BG particles, with the consequent reduction of polymer chain mobility and crystallization kinetics. The intimate contact between the PCL-TES and the inorganic phase can also explain the different morphology displayed by the composite samples after the complete combustion of the polymeric phase in TGA, as reported in Fig. S5 in Supporting Information. In fact, after TGA analysis, the remaining inorganic phase of PCL/BG has a morphology comparable to BGs after the same thermal treatment, for PCL-TES/BG sample the polymer degradation left behind an inorganic phase that displays a more compact and continuous morphology, in line with the hypothesized chemical interaction between PCL-TES and BG.

The involvement of BG in the sol-gel reaction of PCL-TES is further supported by the gel content results. The measurements were carried out on PCL-TES and PCL-TES/BG meshes, both as-spun and post-crosslinked (Table 3). As-spun PCL-TES showed a low gel content (33.4%) which increased to 52% after the thermal treatment. This result is in agreement with previous data that demonstrated that the post-crosslinking treatment was necessary to remarkably increase the gel content, thus the crosslinking degree, to exhibit shape memory properties, keeping at the same time the fibrous morphology, as reported in Fig. S6 [25,26]. Differently, in PCL-TES/BG the gel content was significantly higher (87.1%) just after electrospinning and remained constant after the post-crosslinking. It is thus evident that bioactive glass contributes to reduce the soluble fraction of fibers by promoting hydrolysis and condensation of PCL-TES terminal groups by acting as crosslinking agents, as illustrated in the scheme in Fig. 2.

DSC analysis was also performed to investigate the effect of the crosslinking on the thermal transitions of the scaffolds. The calorimetric heating scan performed at 20 °C/min after a controlled cooling at 10 °C/min is reported in Fig. S7 and the relative calorimetric data are listed in Table S1. It is observed that the melting enthalpy of PCL-TES/BG is not affected by the crosslinking treatment. Conversely, the melting enthalpy of PCL-TES is slightly lower in the crosslinked sample with respect to the corresponding as-spun mat. This result is in line with the significant increase of gel content after thermal treatment for the latter sample.

The shape memory performances of the scaffolds were investigated by applying a conventional cyclic shape memory testing methodology (Fig. 4A reports a representative strain-stress-temperature curve). The cycle consisted in a first "programming step" where the material was kept at 80 °C (above T_m), to melt PCL crystal phase, and deformed at a given level of applied strain, $\varepsilon_{applied}$ (Fig. 4A, step a-b). The "fixing step" followed, where the material was cooled under fixed strain at 0 °C (below polymer T_c, Fig. 4A, step b-c) and the applied strain was fixed thanks to the formation of PCL crystal phase. The load was then removed (Fig. 4A, c-d) and the residual strain at unloading (ε_{unload}) was measured. The final "recovery step" monitored the strain reduction during a heating ramp to temperatures above melting (Fig. 4A, d-e), until a final value of residual stress, ε_{res}, was attained.

This kind of thermo-mechanical cycle was applied to post-crosslinked PCL-TES and PCL-TES/BG mats. The latter was investigated both as spun and after post-crosslinking treatment. Table 4 reports the shape fixity (Equation (3)) and the shape recovery at 80 °C (Equation (4)). For all tested samples, the shape fixity was excellent and the shape recovery was higher than 90% for all samples: PCL-TES/BG post-

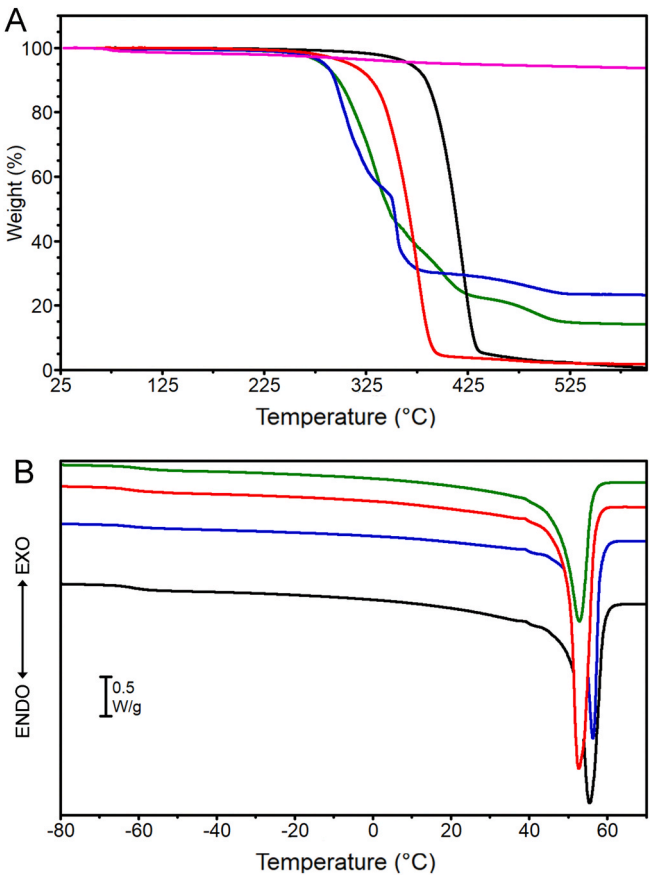

Fig. 3. A) TGA curves of PCL (black), PCL/BG (blue), PCL-TES (red), PCL-TES/BG (green) and BG particles (pink); B) DSC heating scan after cooling of PCL (black), PCL/BG (blue), PCL-TES (red) and PCL-TES/BG (green). (For interpretation of the references to colour in this figure legend, the reader is referred to the Web version of this article.)

Table 2
Calorimetric data of electrospun samples (heating scan performed at 20 °C/min after a controlled cooling at 10 °C/min).

Sample	T_g [°C]	ΔC_p [J/g°C]	T_m [°C]	ΔH_m [J/g]	$\Delta H_{m\text{-}PCL}$ [J/g][a]	χ_c [%][b]
PCL	−61	0.18	55	66	66	49
PCL/BG	−62	0.12	56	47	63	47
PCL-TES	−62	0.20	53	71	71	53
PCL-TES/BG	−59	0.15	53	51	60	44

[a] ΔH_m relative to the weight amount of PCL in the sample.
[b] Calculated by applying Equation (2) reported in the Experimental Section, where f = 1 for PCL and PCL-TES and f = 0.75 for PCL/BG and f = 0.85 for PCL-TES/BG.

Table 3
Gel content of as-spun and crosslinked PCL-TES and PCL-TES/BG.

Sample	G [%][a]
PCL-TES as-spun[b]	33.4 ± 0.6
PCL-TES post-crosslinked[b]	52 ± 1
PCL-TES/BG as-spun[c]	87.1 ± 0.5
PCL-TES/BG post-crosslinked[c]	87.4 ± 0.6

[a] Gel content was calculated according to Equation (1), reported in the Experimental Section.
[b] In Equation (1): $f_{BG} = 0$ and $f_{PCL\text{-}TES} = 1$.
[c] In Equation (1): $f_{BG} = 0.15$ and $f_{PCL\text{-}TES} = 0.85$.

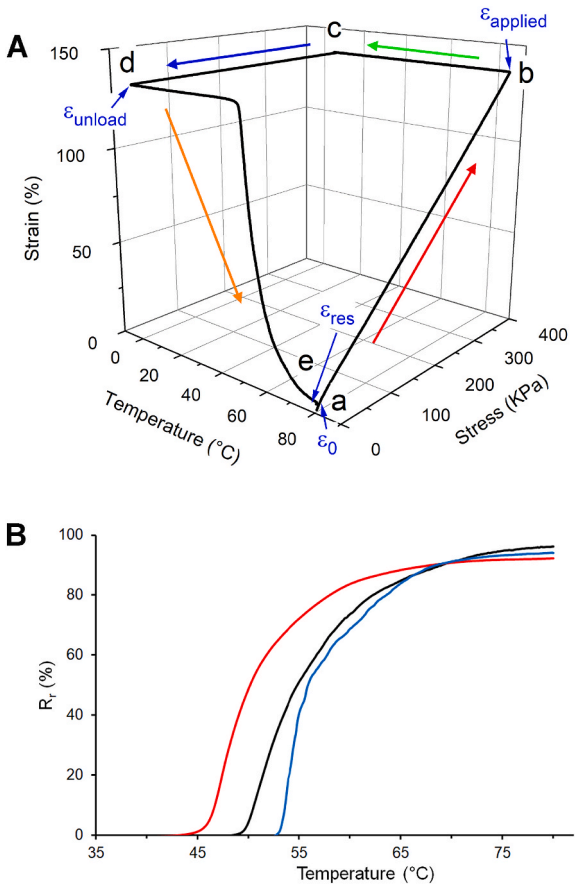

Fig. 4. A) Thermo-mechanical cycle for evaluating shape memory properties: a) sample is kept at 80 °C (above polymer T_m) at a $\varepsilon_0 = 0\%$; a-b deformation stage load control (loading rate: 0.04 N min^{-1}) up to $\varepsilon_{applied}$; b-c cooling under fixed strain; c-d unloading (sample deformation in d is ε_{unload}) and d-e heating and recovery up to ε_{rec}. B) Normalized shape recovery evolution over temperature for the different samples: PCL-TES post-crosslinked (blue), PCL-TES/BG as spun (red) and PCL-TES/BG post-crosslinked (black). (For interpretation of the references to colour in this figure legend, the reader is referred to the Web version of this article.)

Table 4
Shape fixity (R_f) and shape recovery (R_r) capabilities.

Sample	R_f[a]	R_r[b]
PCL-TES post-crosslinked	100%	94%
PCL-TES/BG as-spun	100%	92%
PCL-TES/BG post-crosslinked	100%	96%

[a] Shape fixity was calculated according to Equation (3), reported in the Experimental Section.
[b] Shape recovery was calculated according to Equation (4), reported in the Experimental Section.

crosslinked showed the highest shape recovery (96%), followed by PCL-TES post-crosslinked (94%) and PCL-TES/BG as spun (92%). The excellent shape memory properties displayed by as-spun PCL-TES/BG are worthy of attention: these fibers, due to the presence of BG particles, do not require to be thermally treated to be crosslinked, as previously discussed. Conversely, the as-spun PCL-TES cannot sustain the thermo-mechanical cycle, since when heated at 80 °C it melts losing its fibrous structure, as previously found [25].

The high shape recovery measured for all the tested electrospun samples is not apparently linked to the crosslinking degree, as highlighted by PCL-TES post-crosslinked that, albeit having a gel content of only 52%, showed a shape recovery of 94%. A similar result was

previously reported for such a kind of PCL-based electrospun samples where the deformation applied during the "programming step" promoted a significant fiber alignment and the macroscopic shape recovery was accompanied by a microscopic recovery of the randomly oriented fiber structure [25]. The excellent recovery of both microscopic and macroscopic shapes can be in part ascribed to the presence of fiber "fusion" at contact points that resist the different steps of the thermo-mechanical cycle and prevent fibers from slipping from each other.

Shape recovery as a function of temperature is reported in Fig. 4B. The recovery started from 53 °C, 50 °C and 45 °C for PCL-TES post-crosslinked, PCL-TES/BG post-crosslinked and PCL-TES/BG as spun, respectively. Since the recovery process takes place upon crystal phase melting, it is expected that the onset temperature of recovery is strictly correlated to the onset of melting temperature and to the distribution of crystallite population [29]. The DSC analysis carried out by applying the same thermal program used for shape memory test, indeed, revealed the presence of different crystal populations in the samples under investigation (Fig. S6 in Supporting Information). The melting peaks of PCL-TES/BG as-spun and of PCL-TES post-crosslinked overlap in the low-temperature region but the latter displays a significant fraction of high-melting crystallites, thus requiring the highest temperature for achieving chain mobility and unblocking the temporary shape among the investigated sample. The PCL-TES/BG post-crosslinked shows a melting peak similar to the corresponding as spun fibers but shifted to higher temperatures, in line with the corresponding shift of the shape recovery to higher temperatures.

After immersion in SBF for 7 days, all electrospun samples preserved their fibrillary morphology, as reported in Fig. 5. Moreover, for the PCL/BG and PCL-TES/BG composite meshes it was possible to observe mineralization already after 1 day of immersion (data shown in Fig. S8), which was more evident and homogenous after 7 days of immersion, as reported in Fig. 5B and D. As expected, no deposition on the fiber surface was noticed for PCL and PCL-TES meshes (Fig. 5A and C). Evidence of mineralization in composite electrospun fibers incorporating bioactive glass has been already reported in literature [39,59,60], confirming that the incorporation of BG particles does not affect or inhibit their bioactivity. Usually, mineralization is associated with applications in bone tissue engineering or interface tissue engineering focused on hard-to-soft interfaces (i.e. cartilage-bone, muscle/ligament-bone, etc.), but its suitability also for soft tissue engineering applications is still a topic of discussion in the scientific community [45,61].

EDX analysis was also carried out on composite fibers before and after immersion in SBF solution and results are reported in Fig. 6. Even though it is not possible to use EDX analysis for quantitative evaluation, the information provided about the elemental analysis of the particles inside composite fibers and deposits after immersion, already highlighted in Fig. 5, confirmed the presence and incorporation of BG particles in the polymeric fibers (as-spun), as already shown above by using TEM analysis. After immersion in SBF, the formation of hydroxycarbonate apatite is confirmed for both PCL/BG and PCL-TES/BG samples.

To further investigate the nature of those deposits, FTIR analysis has been performed and the spectra are reported in Fig. 7. FTIR analysis shows that all the spectra (before and after immersion in SBF) present the main bands related to PCL, as previously reported [39]. In the spectra of the as-spun fibers (Fig. 7A) it is possible to detect the presence of the BG particles in both composites because of the wide band centered around 500 cm^{-1}, which could be ascribable to Si–O–Si rocking [62,63]. The immersion in SBF (Fig. 7B) did not modified the FTIR spectra of the neat polymeric fibers (PCL and PCL-TES). Whereas, for what concerns the spectra of both composites fibers, new bands, which could be related to the samples' bioactivity, appeared: absorption peaks at 560 and 600 cm^{-1} can be ascribed to P–O bending vibration in crystalline phosphate [62] and the peaks centered at 875 and 1030 cm^{-1} can be related to CO_3^{2-} bending and Si–OH stretching vibrations, respectively [62]. These bands are typical of BG powders immersed in SBF solution, meaning that the incorporation of the BG particles in the fibers did not affect their bioactivity, which is maintained in the fibers. The combination of EDX and FTIR results enabled to conclude that the precipitates covering the fiber surface are hydroxycarbonate apatite structures, confirming, therefore, the *in vitro* bioactivity conferred by the BG particles to PCL-based composite meshes. Concerning the evolution of the formation of this hydroxycarbonate apatite layer, in Figs. S8A and C it is possible to observe the morphology after one day of immersion in SBF, in comparison with the analysis provided for the samples after 7 days of immersion (Figs. 5 and 6). Moreover, the FTIR spectra in Figs. S8B and D reported the evolution of the peaks related to the mineralization and the progressive increase of the bands related to phosphate and carbonate groups centered at 1030, 875, 560 and 600 cm^{-1}.

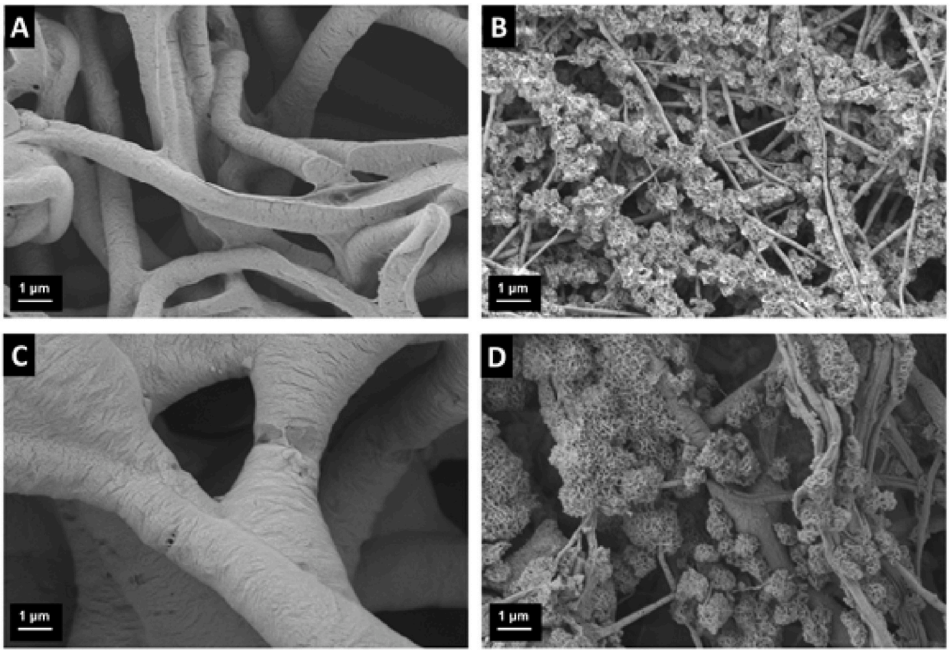

Fig. 5. SEM images of electrospun meshes after 7 days of incubation in simulated body fluid. (A) PCL, (B) PCL/BG, (C) PCL-TES, (D) PCL-TES/BG. Scale bar = 1 µm.

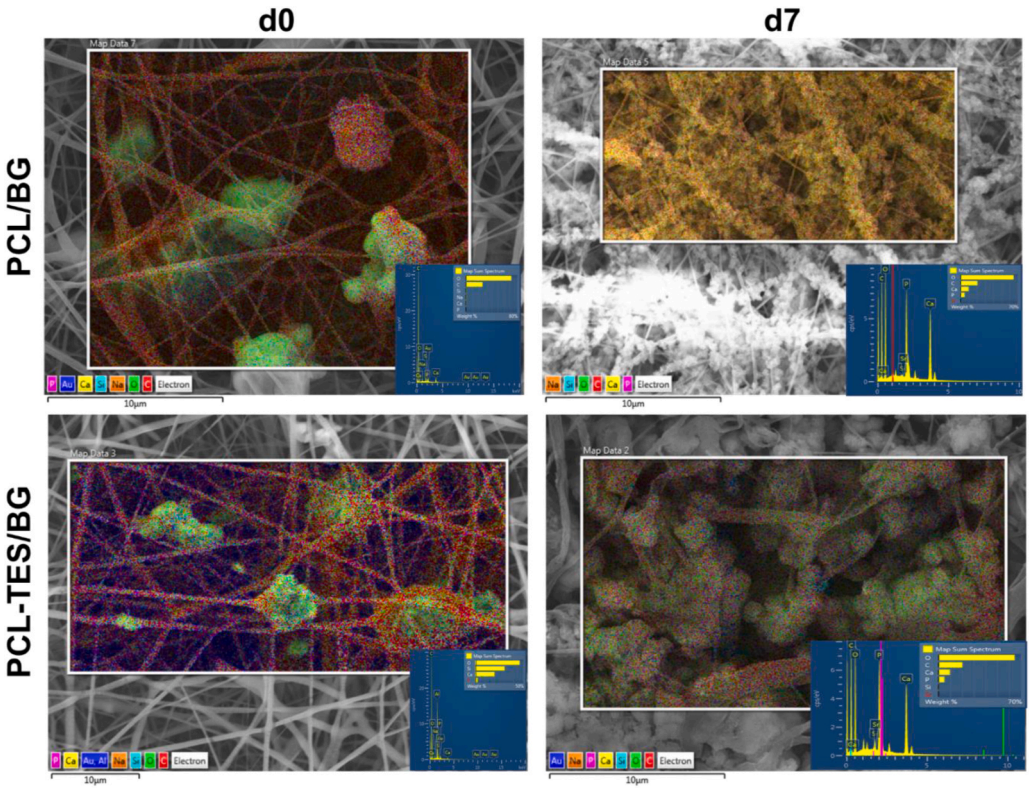

Fig. 6. SEM/EDX analysis on PCL/BG and PCL-TES/BG samples before (d0) and after 7 days (d7) of immersion in SBF. Scale bar = 10 µm.

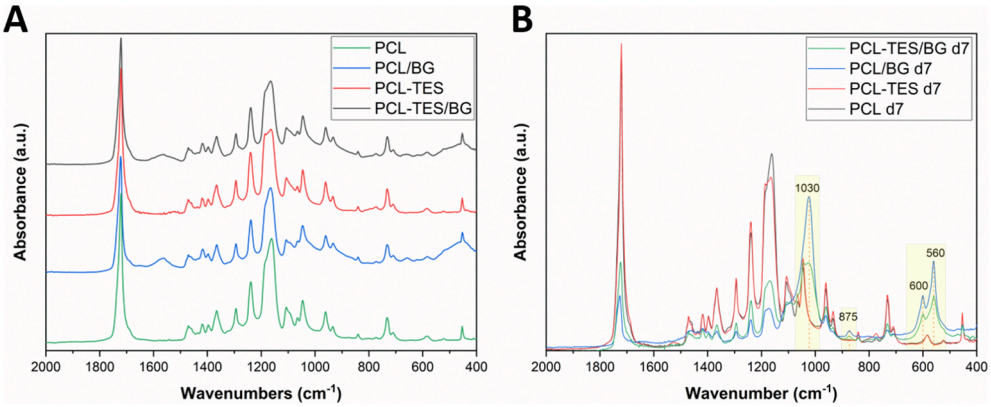

Fig. 7. FTIR analysis of PCL, PCL-TES, PCL/BG and PCL-TES/BG fibers as-spun (A) and after 7 days of immersion in SBF (B). Main peaks indicated on the spectra are discussed in the text.

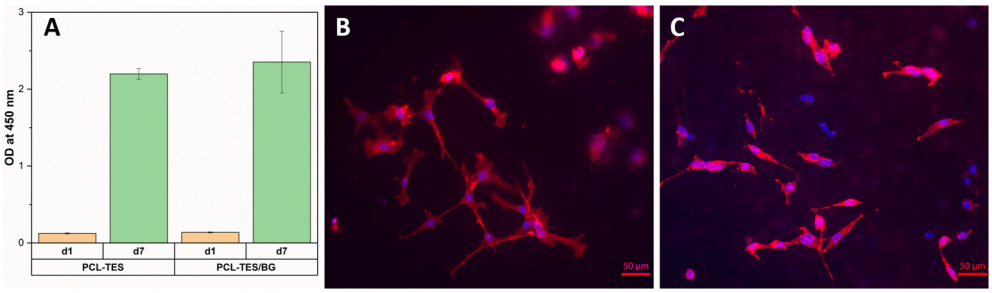

Fig. 8. (A) WST-8 assay results: OD at 450 nm after 1 and 7 days from cell seeding; (B,C) cell nuclei (blue, DAPI) and cytoskeleton (red, rhodamine phalloidin) of ST-2 cells on PCL-TES (B) and PCL-TES/BG (C) 7 days after seeding. Scale bar = 50 µm. (For interpretation of the references to colour in this figure legend, the reader is referred to the Web version of this article.)

Respect to other composite electrospun fibers incorporating bioactive glass, it is worth to notice that the BG particles were not released upon immersion in SBF, as reported in Ref. [41], being able to show the formation of a hydroxycarbonate apatite layer. This property, added to the shape memory one, highlights the novelty of this work and the potential of the novel fiber mats for future applications.

Preliminary cytocompatibility tests have been carried out on PCL-TES and PCL-TES/BG mats and the obtained results are reported in Fig. 8. From the evaluation of the values of the optical density (OD) at 450 nm, it is possible to observe that comparable values have been obtained for the two samples at both time points, demonstrating that the addition of bioactive glass particles and the released ions do not affect or inhibit cell viability. Moreover, for both samples cell proliferation could be evaluated considering the ratio obtained by dividing the average OD value at the time point d7 by the same value at d1. These ratios, 17.7 and 17.1 for PCL-TES and PCL-TES/BG, respectively, are quite high if compared with the same ratio calculated for other PCL-based composite electrospun fibers [41]. Also, the cell morphology reported in Fig. 8B and C shows a comparable distribution of cells, which appeared elongated in both electrospun mats.

4. Conclusion

In this work, nanocomposite electrospun fibers with excellent shape memory properties have been successfully obtained by using PCL-TES and bioactive glass particles. The hybrid PCL-TES/BG nanostructure was designed to provide bioactivity to the polymeric shape memory material, and at the same time, to exploit the formation of chemical interactions between the silanol groups at the particle surface and PCL-TES chain ends to improve crosslinking with respect to plain PCL-TES. Fiber characterization was firstly focused at confirming and investigating the incorporation of BG particles in the electrospun fibers. Characterization of the shape memory properties demonstrated that for all tested samples excellent shape fixity and shape recovery higher than 90% were obtained. It is worth noting that PCL-TES/BG showed remarkable shape memory parameters even in the absence of further post-crosslinking treatment due to the presence of BG particles. Evidence of mineralization in PCL/BG and PCL-TES/BG composite electrospun fibers confirmed that BG particles confer *in vitro* bioactivity to PCL-based nanocomposite fibers. The addition of BG particles to PCL-based polymer fibers maintains cytocompatibility and it does not inhibit ST-2 cell viability. The fabrication of fibrous nanocomposites reported in this work has been demonstrated to be a simple but powerful tool to obtain biomimetic and biocompatible materials with attractive shape memory behavior, combined with bioactivity, suitable for bone and soft tissue engineering applications.

CRediT authorship contribution statement

Liliana Liverani: Conceptualization, Methodology, Formal analysis, Investigation, Writing – original draft. **Anna Liguori:** Methodology, Formal analysis, Investigation, Writing – original draft. **Paola Zezza:** Formal analysis, Investigation. **Chiara Gualandi:** Formal analysis, Investigation, Writing – review & editing. **Maurizio Toselli:** Formal analysis, Writing – review & editing. **Aldo R. Boccaccini:** Conceptualization, Resources, Writing – review & editing, Supervision. **Maria Letizia Focarete:** Conceptualization, Resources, Writing – review & editing, Supervision.

Declaration of competing interest

The authors declare no conflict of interest.

Acknowledgements

The Italian Ministry of University and Research (MIUR) is acknowledged. The University of Bologna is acknowledged for the scholarship awarded to P.Z.

Appendix A. Supplementary data

Supplementary data to this article can be found online at https://doi.org/10.1016/j.bioactmat.2021.09.020.

References

[1] Y. Xia, Y. He, F. Zhang, Y. Liu, J. Leng, A review of shape memory polymers and composites: mechanisms, materials, and applications, Adv. Mater. 33 (2021) 2000713, https://doi.org/10.1002/ADMA.202000713.
[2] M. Behl, M.Y. Razzaq, A. Lendlein, Multifunctional shape-memory polymers, Adv. Mater. 22 (2010) 3388–3410, https://doi.org/10.1002/ADMA.200904447.
[3] H. Meng, G. Li, A review of stimuli-responsive shape memory polymer composites, Polymer 54 (2013) 2199–2221, https://doi.org/10.1016/J.POLYMER.2013.02.023.
[4] R. Xiao, W.M. Huang, Heating/solvent responsive shape-memory polymers for implant biomedical devices in minimally invasive surgery: current status and challenge, Macromol. Biosci. 20 (2020) 2000108, https://doi.org/10.1002/MABI.202000108.
[5] W. Zhao, L. Liu, F. Zhang, J. Leng, Y. Liu, Shape memory polymers and their composites in biomedical applications, Mater. Sci. Eng. C 97 (2019) 864–883, https://doi.org/10.1016/j.msec.2018.12.054.
[6] A. Lendlein, M. Behl, B. Hiebl, C. Wischke, Shape-memory polymers as a technology platform for biomedical applications, Expet Rev. Med. Dev. 7 (2010) 357–379, https://doi.org/10.1586/erd.10.8.
[7] B.Q.Y. Chan, Z.W.K. Low, S.J.W. Heng, S.Y. Chan, C. Owh, X.J. Loh, Recent advances in shape memory soft materials for biomedical applications, ACS Appl. Mater. Interfaces 8 (2016) 10070–10087, https://doi.org/10.1021/ACSAMI.6B01295.
[8] Y.-J. Kim, Y.T. Matsunaga, Thermo-responsive polymers and their application as smart biomaterials, J. Mater. Chem. B. 5 (2017) 4307–4321, https://doi.org/10.1039/C7TB00157F.
[9] D. Zhang, O.J. George, K.M. Petersen, A.C. Jimenez-Vergara, M.S. Hahn, M. A. Grunlan, A bioactive "self-fitting" shape memory polymer scaffold with potential to treat cranio-maxillo facial bone defects, Acta Biomater. 10 (2014) 4597–4605, https://doi.org/10.1016/j.actbio.2014.07.020.
[10] M. Bao, X. Lou, Q. Zhou, W. Dong, H. Yuan, Y. Zhang, Electrospun biomimetic fibrous scaffold from shape memory polymer of PDLLA- co -TMC for bone tissue engineering, ACS Appl. Mater. Interfaces 6 (2014) 2611–2621, https://doi.org/10.1021/am405101k.
[11] R.M. Baker, L.F. Tseng, M.T. Iannolo, M.E. Oest, J.H. Henderson, Self-deploying shape memory polymer scaffolds for grafting and stabilizing complex bone defects: a mouse femoral segmental defect study, Biomaterials 76 (2016) 388–398, https://doi.org/10.1016/j.biomaterials.2015.10.064.
[12] C.O. Correia, Á.J. Leite, J.F. Mano, Chitosan/bioactive glass nanoparticles scaffolds with shape memory properties, Carbohydr. Polym. 123 (2015) 39–45, https://doi.org/10.1016/j.carbpol.2014.12.076.
[13] X. Hu, J. He, X. Yong, J. Lu, J. Xiao, Y. Liao, Q. Li, C. Xiong, Biodegradable poly (lactic acid-co-trimethylene carbonate)/chitosan microsphere scaffold with shape-memory effect for bone tissue engineering, Colloids Surf. B Biointerfaces 195 (2020) 111218, https://doi.org/10.1016/j.colsurfb.2020.111218.
[14] H. Xuan, H. Hu, C. Geng, J. Song, Y. Shen, D. Lei, Q. Guan, S. Zhao, Z. You, Biofunctionalized chondrogenic shape-memory ternary scaffolds for efficient cell-free cartilage regeneration, Acta Biomater. 105 (2020) 97–110, https://doi.org/10.1016/j.actbio.2020.01.015.
[15] C.M. Yakacki, R. Shandas, C. Lanning, B. Rech, A. Eckstein, K. Gall, Unconstrained recovery characterization of shape-memory polymer networks for cardiovascular applications, Biomaterials 28 (2007) 2255–2263, https://doi.org/10.1016/j.biomaterials.2007.01.030.
[16] M. Montgomery, S. Ahadian, L. Davenport Huyer, M. Lo Rito, R.A. Civitarese, R. D. Vanderlaan, J. Wu, L.A. Reis, A. Momen, S. Akbari, A. Pahnke, R.K. Li, C. A. Caldarone, M. Radisic, Flexible shape-memory scaffold for minimally invasive delivery of functional tissues, Nat. Mater. 16 (2017) 1038–1046, https://doi.org/10.1038/nmat4956.
[17] W. Zhao, L. Liu, F. Zhang, J. Leng, Y. Liu, Shape memory polymers and their composites in biomedical applications, Mater. Sci. Eng. C 97 (2019) 864–883, https://doi.org/10.1016/J.MSEC.2018.12.054.
[18] M. Bil, E. Kijeńska-Gawrońska, E. Głodkowska-Mrówka, A. Manda-Handzlik, P. Mrówka, Design and in vitro evaluation of electrospun shape memory polyurethanes for self-fitting tissue engineering grafts and drug delivery systems, Mater. Sci. Eng. C 110 (2020) 110675, https://doi.org/10.1016/j.msec.2020.110675.
[19] Y. Wang, Y. Miao, J. Zhang, J.P. Wu, T.B. Kirk, J. Xu, D. Ma, W. Xue, Three-dimensional printing of shape memory hydrogels with internal structure for drug delivery, Mater. Sci. Eng. C 84 (2018) 44–51, https://doi.org/10.1016/j.msec.2017.11.025.
[20] C. Wischke, A.T. Neffe, A. Lendlein, Controlled drug release from biodegradable shape-memory polymers, in: A. Lendlein (Ed.), Shape-Memory Polym, Springer Berlin Heidelberg, Berlin, Heidelberg, 2010, pp. 177–205, https://doi.org/10.1007/12_2009_29.

[21] S. Di, X. Liu, D. Liu, T. Gong, L. Lu, S. Zhou, A multifunctional porous scaffold with capacities of minimally invasive implantation, self-fitting and drug delivery, Mater. Today Chem. 1–2 (2016) 52–62, https://doi.org/10.1016/j.mtchem.2016.11.004.
[22] J. Wang, H. Gao, Y. Hu, N. Zhang, W. Zhou, C. Wang, B.P. Binks, Z. Yang, 3D printing of Pickering emulsion inks to construct poly(D,L-lactide-co-trimethylene carbonate)-based porous bioactive scaffolds with shape memory effect, J. Mater. Sci. 56 (2021) 731–745, https://doi.org/10.1007/s10853-020-05318-7.
[23] Y. Zhang, J. Hu, R. Xie, Y. Yang, J. Cao, Y. Tu, Y. Zhang, T. Qin, X. Zhao, A programmable, fast-fixing, osteo-regenerative, biomechanically robust bone screw, Acta Biomater. 103 (2020) 293–305, https://doi.org/10.1016/j.actbio.2019.12.017.
[24] X. Wu, S. Mahalingam, S.K. VanOosten, C. Wisdom, C. Tamerler, M. Edirisinghe, New generation of tunable bioactive shape memory mats integrated with genetically engineered proteins, Macromol. Biosci. 17 (2017) 1600270, https://doi.org/10.1002/mabi.201600270.
[25] A. Merlettini, S. Pandini, S. Agnelli, C. Gualandi, K. Paderni, M. Messori, M. Toselli, M.L. Focarete, Facile fabrication of shape memory poly(ε-caprolactone) non-woven mat by combining electrospinning and sol-gel reaction, RSC Adv. 6 (2016) 43964–43974, https://doi.org/10.1039/c6ra05490k.
[26] S. Pandini, S. Agnelli, A. Merlettini, F. Chiellini, C. Gualandi, K. Paderni, M. L. Focarete, M. Messori, M. Toselli, Mutifunctional electrospun nonwoven mats with two-way shape memory behavior prepared from sol-gel crosslinked poly (ε-caprolactone), Macromol. Mater. Eng. 302 (2017) 1600519, https://doi.org/10.1002/mame.201600519.
[27] M. Sabzi, M. Ranjbar-Mohammadi, Q. Zhang, S. Kargozar, J. Leng, T. Akhtari, R. Abbasi, Designing triple-shape memory polymers from a miscible polymer pair through dual-electrospinning technique, J. Appl. Polym. Sci. 136 (2019) 47471, https://doi.org/10.1002/app.47471.
[28] F. Zhang, Z. Zhang, T. Zhou, Y. Liu, J. Leng, Shape memory polymer nanofibers and their composites: electrospinning, structure, performance, and applications, Front. Mater. 2 (2015) 62, https://doi.org/10.3389/fmats.2015.00062.
[29] A. Merlettini, M. Gigli, M. Ramella, C. Gualandi, M. Soccio, F. Boccafoschi, A. Munari, N. Lotti, M.L. Focarete, Thermal annealing to modulate the shape memory behavior of a biobased and biocompatible triblock copolymer scaffold in the human body temperature range, Biomacromolecules 18 (2017) 2499–2508, https://doi.org/10.1021/acs.biomac.7b00644.
[30] Á.J. Leite, S.G. Caridade, J.F. Mano, Synthesis and characterization of bioactive biodegradable chitosan composite spheres with shape memory capability, J. Non-Cryst. Solids 432 (2016) 158–166, https://doi.org/10.1016/j.jnoncrysol.2015.04.011.
[31] W.J. Hendrikson, J. Rouwkema, F. Clementi, C.A. Van Blitterswijk, S. Farè, L. Moroni, Towards 4D printed scaffolds for tissue engineering: exploiting 3D shape memory polymers to deliver time-controlled stimulus on cultured cells, Biofabrication 9 (2017), 031001, https://doi.org/10.1088/1758-5090/aa8114.
[32] D. Il Cha, H.Y. Kim, K.H. Lee, Y.C. Jung, J.W. Cho, B.C. Chun, Electrospun nonwovens of shape-memory polyurethane block copolymers, J. Appl. Polym. Sci. 96 (2005) 460–465, https://doi.org/10.1002/app.21467.
[33] H. Zhuo, J. Hu, S. Chen, Electrospun polyurethane nanofibres having shape memory effect, Mater. Lett. 62 (2008) 2074–2076, https://doi.org/10.1016/j.matlet.2007.11.018.
[34] J.N. Zhang, Y.M. Ma, J.J. Zhang, D. Xu, Q.L. Yang, J.G. Guan, X.Y. Cao, L. Jiang, Microfiber SMPU film affords quicker shape recovery than the bulk one, Mater. Lett. 65 (2011) 3639–3642, https://doi.org/10.1016/j.matlet.2011.06.083.
[35] H. Matsumoto, T. Ishiguro, Y. Konosu, M. Minagawa, A. Tanioka, K. Richau, K. Kratz, A. Lendlein, Shape-memory properties of electrospun non-woven fabrics prepared from degradable polyesterurethanes containing poly (ω-pentadecalactone) hard segments, Eur. Polym. J. 48 (2012) 1866–1874, https://doi.org/10.1016/j.eurpolymj.2012.07.008.
[36] S. Neuss, I. Blomenkamp, R. Stainforth, D. Boltersdorf, M. Jansen, N. Butz, A. Perez-Bouza, R. Knüchel, The use of a shape-memory poly(ε-caprolactone) dimethacrylate network as a tissue engineering scaffold, Biomaterials 30 (2009) 1697–1705, https://doi.org/10.1016/j.biomaterials.2008.12.027.
[37] S. Agarwal, A. Greiner, On the way to clean and safe electrospinning-green electrospinning: emulsion and suspension electrospinning, Polym. Adv. Technol. 22 (2011) 372–378, https://doi.org/10.1002/pat.1883.
[38] L. Liverani, M.S. Killian, A.R. Boccaccini, Fibronectin functionalized electrospun fibers by using benign solvents: best way to achieve effective functionalization, Front. Bioeng. Biotechnol. 7 (2019) 68, https://doi.org/10.3389/FBIOE.2019.00068.
[39] L. Liverani, A. Boccaccini, Versatile production of poly(epsilon-caprolactone) fibers by electrospinning using benign solvents, Nanomaterials 6 (2016) 75, https://doi.org/10.3390/nano6040075.
[40] L. Liverani, J. Lacina, J.A. Roether, E. Boccardi, M.S. Killian, P. Schmuki, D. W. Schubert, A.R. Boccaccini, Incorporation of bioactive glass nanoparticles in electrospun PCL/chitosan fibers by using benign solvents, Bioact. Mater. 3 (2018) 55–63, https://doi.org/10.1016/j.bioactmat.2017.05.003.
[41] M. Luginina, K. Schuhladen, R. Orrú, G. Cao, A.R. Boccaccini, L. Liverani, Electrospun PCL/PGS composite fibers incorporating bioactive glass particles for soft tissue engineering applications, Nanomaterials 10 (2020) 978, https://doi.org/10.3390/nano10050978.
[42] L.L. Hench, The story of Bioglass, J. Mater. Sci. Mater. Med. 17 (2006) 967–978, https://doi.org/10.1007/s10856-006-0432-z.
[43] L.L. Hench, R.J. Splinter, W.C. Allen, T.K. Greenlee, Bonding mechanisms at the interface of ceramic prosthetic materials, J. Biomed. Mater. Res. 5 (1971) 117–141, https://doi.org/10.1002/jbm.820050611.
[44] L.L. Hench, Bioactive materials: the potential for tissue regeneration, J. Biomed. Mater. Res. 41 (1998) 511–518, https://doi.org/10.1002/(SICI)1097-4636(19980915)41:4<511::AID-JBM1>3.0.CO;2-F.
[45] V. Miguez-Pacheco, L.L. Hench, A.R. Boccaccini, Bioactive glasses beyond bone and teeth: emerging applications in contact with soft tissues, Acta Biomater. 13 (2015) 1–15, https://doi.org/10.1016/j.actbio.2014.11.004.
[46] A. Hoppe, N.S. Güldal, A.R. Boccaccini, A review of the biological response to ionic dissolution products from bioactive glasses and glass-ceramics, Biomaterials 32 (2011) 2757–2774, https://doi.org/10.1016/j.biomaterials.2011.01.004.
[47] X. Li, J. Shi, X. Dong, L. Zhang, H. Zeng, A mesoporous bioactive glass/polycaprolactone composite scaffold and its bioactivity behavior, J. Biomed. Mater. Res. 84A (2008) 84–91, https://doi.org/10.1002/JBM.A.31371.
[48] K.T. Shalumon, S. Sowmya, D. Sathish, K.P. Chennazhi, S.V. Nair, R. Jayakumar, Effect of incorporation of nanoscale bioactive glass and hydroxyapatite in PCL/chitosan nanofibers for bone and periodontal tissue engineering, J. Biomed. Nanotechnol. 9 (2013) 430–440, https://doi.org/10.1166/JBN.2013.1559.
[49] K. Paderni, S. Pandini, S. Passera, F. Pilati, M. Toselli, M. Messori, Shape-memory polymer networks from sol-gel cross-linked alkoxysilane-terminated poly (ε-caprolactone), J. Mater. Sci. 47 (2012) 4354–4362, https://doi.org/10.1007/s10853-012-6289-2.
[50] J. Schindelin, I. Arganda-Carreras, E. Frise, V. Kaynig, M. Longair, T. Pietzsch, S. Preibisch, C. Rueden, S. Saalfeld, B. Schmid, J.Y. Tinevez, D.J. White, V. Hartenstein, K. Eliceiri, P. Tomancak, A. Cardona, Fiji: an open-source platform for biological-image analysis, Nat. Methods 9 (2012) 676–682, https://doi.org/10.1038/nmeth.2019.
[51] R.L. Miller, Crystallographic data for various polymers, in: Polymer Ha, John Wiley & Sons, Inc., new york, 1992.
[52] F. Fang, H. Wang, H. Wang, W.M. Huang, Y. Chen, N. Cai, X. Chen, X. Chen, Stimulus-responsive shrinkage in electrospun membranes: fundamentals and control, Micromachines 12 (2021) 920, https://doi.org/10.3390/MI12080920, 12 (2021) 920.
[53] T. Kokubo, H. Takadama, How useful is SBF in predicting in vivo bone bioactivity? Biomaterials 27 (2006) 2907–2915, https://doi.org/10.1016/J.BIOMATERIALS.2006.01.017.
[54] A. Yamaguchi, T. Komori, T. Suda, Regulation of osteoblast differentiation mediated by bone morphogenetic proteins, hedgehogs, and Cbfa1, Endocr. Rev. 21 (2000) 393–411, https://doi.org/10.1210/edrv.21.4.0403.
[55] L. Tian, F. Zheng, Z. Li, H. Wang, H. Yuan, X. Zhang, Z. Ma, X. Li, X. Gao, B. Wang, miR-148a-3p regulates adipocyte and osteoblast differentiation by targeting lysine-specific demethylase 6b, Gene 627 (2017) 32–39, https://doi.org/10.1016/j.gene.2017.06.002.
[56] D. Hamam, D. Ali, M. Kassem, A. Aldahmash, N.M. Alajez, Micrornas as regulators of adipogenic differentiation of mesenchymal stem cells, Stem Cell. Dev. 24 (2015) 417–425, https://doi.org/10.1089/scd.2014.0331.
[57] O. Persenaire, M. Alexandre, P. Degée, P. Dubois, Mechanisms and kinetics of thermal degradation of poly(ε-caprolactone), Biomacromolecules 2 (2001) 288–294, https://doi.org/10.1021/bm0056310.
[58] A. Larrañaga, J.R. Sarasua, Effect of bioactive glass particles on the thermal degradation behaviour of medical polyesters, Polym. Degrad. Stabil. 98 (2013) 751–758, https://doi.org/10.1016/j.polymdegradstab.2012.12.015.
[59] H.H. Lee, H.S. Yu, J.H. Jang, H.W. Kim, Bioactivity improvement of poly (ε-caprolactone) membrane with the addition of nanofibrous bioactive glass, Acta Biomater. 4 (2008) 622–629, https://doi.org/10.1016/j.actbio.2007.10.013.
[60] H.M. Lin, Y.H. Lin, F.Y. Hsu, Preparation and characterization of mesoporous bioactive glass/polycaprolactone nanofibrous matrix for bone tissues engineering, J. Mater. Sci. Mater. Med. 23 (2012) 2619–2630, https://doi.org/10.1007/s10856-012-4734-z.
[61] S. Naseri, W.C. Lepry, S.N. Nazhat, Bioactive glasses in wound healing: hope or hype? J. Mater. Chem. B. 5 (2017) 6167–6174, https://doi.org/10.1039/c7tb01221g.
[62] K. Zheng, A. Solodovnyk, W. Li, O.-M. Goudouri, C. Stähli, S.N. Nazhat, A. R. Boccaccini, Aging time and temperature effects on the structure and bioactivity of gel-derived 45S5 glass-ceramics, J. Am. Ceram. Soc. 98 (2015) 30–38, https://doi.org/10.1111/jace.13258.
[63] M. Cerruti, D. Greenspan, K. Powers, Effect of pH and ionic strength on the reactivity of Bioglass® 45S5, Biomaterials 26 (2005) 1665–1674, https://doi.org/10.1016/j.biomaterials.2004.07.009.